

## Photoexcitation-Induced Nonthermal Ultrafast Loss of Long-Range Order in GeTe

Liqiu Yang, Subodh C. Tiwari, Shogo Fukushima, Fuyuki Shimojo, Rajiv K. Kalia, Aiichiro Nakano, Priya Vashishta, and Paulo S. Brancio\*



Cite This: *J. Phys. Chem. Lett.* 2022, 13, 10230–10236



Read Online

ACCESS |

Metrics & More

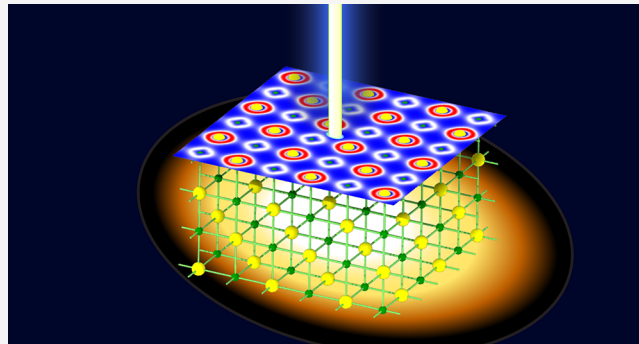


Article Recommendations



Supporting Information

**ABSTRACT:** Nonadiabatic quantum molecular dynamics is used to investigate the evolution of GeTe photoexcited states. Results reveal a photoexcitation-induced picosecond nonthermal path for the loss of long-range order. A valence electron excitation threshold of 4% is found to trigger local disorder by switching Ge atoms from octahedral to tetrahedral sites and promoting Ge–Ge bonding. The resulting loss of long-range order for a higher valence electron excitation fraction is achieved without fulfilling the Lindemann criterion for melting, therefore utilizing a nonthermal path. The photoexcitation-induced structural disorder is accompanied by charge transfer from Te to Ge, Ge–Te bonding-to-antibonding, and Ge–Ge antibonding-to-bonding change, triggering Ge–Te bond breaking and promoting the formation of Ge–Ge wrong bonds. These results provide an electronic-structure basis to understand the photoexcitation-induced ultrafast changes in the structure and properties of GeTe and other phase-change materials.



In contrast with the crystalline phase, which is characterized by the presence of resonance bonding,<sup>13–15</sup> the amorphous phase in PCMs displays primarily covalent bonding. In GeTe, while some Ge atoms preserve a local structure similar to that of the crystalline phase,<sup>16–18</sup> which is referred to as “defective octahedral sites” or “pyramidal sites”, most Ge atoms acquire a tetrahedral bonding geometry, characterized by four equivalent Ge–Te bonds forming 109.5° bond angles in a typical  $sp^3$  hybridization.<sup>19</sup> This raises the question about the formation mechanism of this tetrahedral geometry and the coexistence of octahedral- and tetrahedral-like sites in the amorphous phase.<sup>20–23</sup>

The effect of laser pulses on a solid may not be described simply as a “heating effect” when the induced repulsive interatomic forces swiftly induce lattice disorder. That is the case when the laser pulse is intense and the duration is as short as femtoseconds, which can generate effects on a time scale significantly below the characteristic phonon relaxation time.<sup>24</sup> Nonetheless, the photoexcitation-induced nonthermal bond changes in GeTe leading to amorphization are not fully

Phase-change materials (PCMs) exhibit remarkable differences in the resistivity of their crystalline and amorphous phases, which can be used to construct effective nonvolatile memory devices.<sup>1</sup> The  $(\text{GeTe})_x(\text{Sb}_2\text{Te}_3)_{1-x}$  alloy family (GST) shows nanosecond fast crystalline–amorphous phase transition and is the most promising and studied PCM.<sup>1–5</sup> The amorphous phase of PCMs is conventionally obtained by melting the crystalline materials, by application of short laser or electric pulses, followed by quenching to room temperature. Alternatively, it has been reported that femtosecond laser photoexcitation can induce a nonthermal amorphization process.<sup>6–8</sup> Using first-principles molecular dynamics (MD), Li et al.<sup>8</sup> showed that a 9% electronic excitation leads to amorphization of GST within several picoseconds at a temperature below 700 K. Tiwari et al.<sup>8</sup> demonstrated ultrafast nonthermal amorphization in  $\text{Sb}_2\text{Te}_3$  induced by photoexcitation. Experimental reports also confirm ultrafast photoexcitation-driven phase-change in GST alloys.<sup>9</sup>

GeTe is a prototype binary PCM in the GST alloy family, capable of switching rapidly between its vacancy-free crystalline structure and its amorphous phase.<sup>10,11</sup> At low temperatures, GeTe is known to adopt a bond hierarchy, where short and long Ge–Te bonds indicate strong and weak bonding in a Peierls distorted rock salt structure.<sup>12</sup> Kolobov et al.<sup>6</sup> demonstrated that small atomic misalignment could trigger the destruction of the subsystem of weaker bonds in GeTe and subsequent collapse of the ordered phase leading to nonthermal amorphization.

Received: August 6, 2022

Accepted: October 13, 2022



ACS Publications

© XXXX American Chemical Society

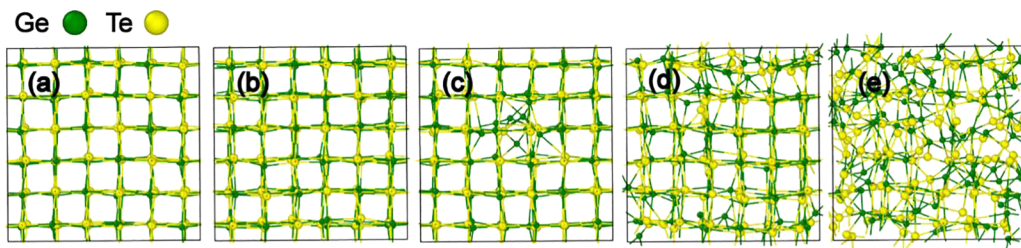


**Figure 1.** Changes in the structure of GeTe with photoexcitation. (a) GeTe structure after thermalization at 300 K. (b–e) GeTe structures after 5 ps of photoexcitation at different excitation levels  $n$ :  $n = 2.6\%$  (b), 4.0% (c), 5.2% (d), and 7.5% (e). Green and yellow spheres represent Ge and Te atoms, respectively.

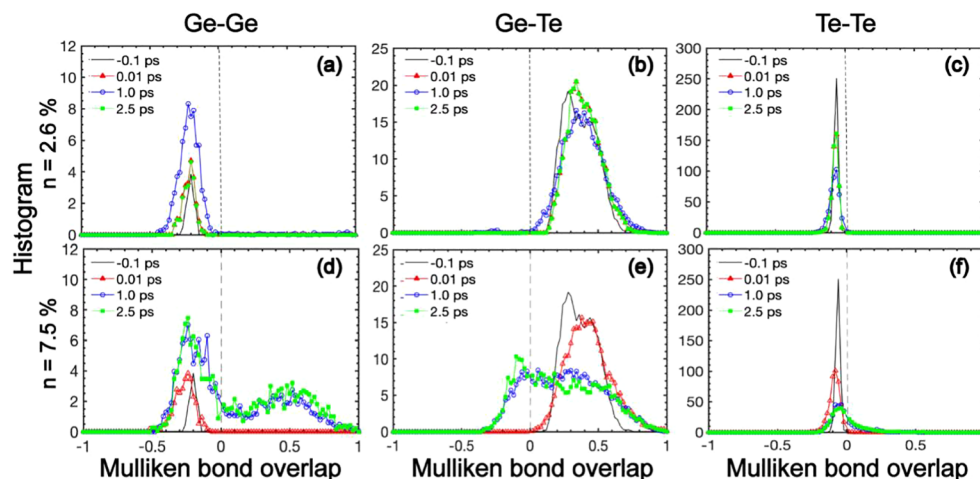


**Figure 2.** Mulliken bond overlap as a function of time for Ge–Ge, Ge–Te, and Te–Te bonds. The black curve corresponds to time  $t = -0.1$  ps (before photoexcitation). Red, blue, and green curves represent results at  $t = 0.01, 1.0$ , and 2.5 ps (after photoexcitation), respectively.

understood. Possible mechanisms, such as the phase flip of the wave function<sup>24</sup> and the formation of transient three-center bonds,<sup>25</sup> have been proposed and need to be further validated. In addition, no direct investigation of the evolution of the GeTe structure with excited states leading to the loss of long-range order induced by photoexcitation has been performed so far to validate these views.

Here, we apply nonadiabatic quantum molecular dynamics (NAQMD) simulations to investigate the evolution of the GeTe structure with photoexcited states. NAQMD simulations show disorder in GeTe via a nonthermal path within a few picoseconds when the photoexcitation level exceeds 4.0% of the valence electrons. The simulation results provide insights into the onset of the local disorder and the change in the GeTe bonding nature, preceding the nonthermal ultrafast loss of long-range crystalline order.

In the GeTe cubic crystalline phase, each atom has a coordination number of six and displays an octahedral atomic arrangement typical of rocksalt structures with cation/anion sites occupied by Ge/Te atoms, respectively.<sup>26</sup> Figure 1a shows the thermalized GeTe structure at 300 K, along with GeTe structures at 700 K after 5 ps of photoexcitation at different levels of excitation. NAQMD simulations are performed with  $n = 2.6\%$ , 4.0%, 5.2%, and 7.5% valence electrons excited. The GeTe structure relaxed at 300 K shows a broader Ge–Te bond length peak, as shown in Figure S1, which can be explained by Peierls distortions (PDs).<sup>12,20,27–30</sup> The distortion occurs along the [111] direction and was reported to lower the electronic energy (44 meV/atom) and increase the band gap<sup>31</sup> from 0.37 to 0.5 eV. In our simulations

at 300 K, the thermal vibration destroys the well-defined arrangement of long and short bond lengths, and instead, the bond length distribution displays a broad distribution around  $\sim 3$  Å (Figure S1). As shown in Figure 1b, excitation at  $n = 2.6\%$  is insufficient to induce structural disorder. However, for photoexcitation at  $n = 4.0\%$ , the results show local disorder, indicating that the threshold to trigger GeTe local disorder is achieved. A higher excitation level leads to extensive disorder, widespread loss of the long-range crystalline order, and the formation of Ge–Ge and Te–Te wrong bonds.

In order to characterize the structural change illustrated in Figure 1, the mean square displacement (MSD) of Ge atoms is calculated as a function of time (Figure S2a), while the evolution of the fraction of Ge–Ge and Te–Te “wrong” bonds is plotted in Figure S2b. The induced atomic diffusion leads to widespread bond breaking and loss of long-range order. It should be noted that such an amorphization takes place without any melting as the temperature of the system is kept at 700 K, well below the melting point (at  $\sim 1000$  K). That implies that by applying femtosecond laser photoexcitation, the crystalline-to-amorphous transition time could be reduced from hundreds to a few picoseconds using a nonthermal path.

The overall evolution of the excited electronic state is provided by the calculated Mulliken bond overlap as a function of time. Results for excitation at  $n = 2.6\%$  and 7.5% are shown in Figure 2. Before photoexcitation at time  $t = -0.1$  ps, Ge–Ge and Te–Te bond pairs are in antibonding states with peaks at  $-0.2$  and  $-0.08$ , respectively. Meanwhile, the Ge–Te bond pair is in a bonding state as expected, with a peak at 0.25. For 2.6% excitation, at all times, the Ge–Ge, Ge–Te, and Te–Te

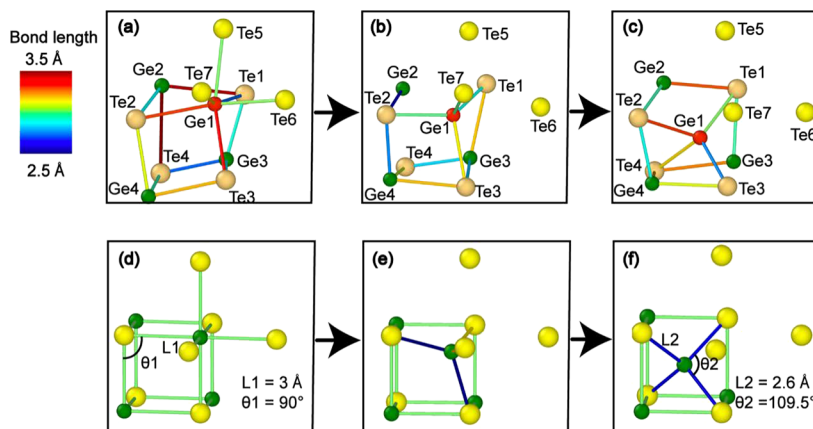


**Figure 3.** Local disorder triggered by Ge diffusion at  $n = 4.0\%$ . (a–c) Shift of Ge atom from octahedral to tetrahedral sites for  $t = 1.833$  ps (a),  $2.094$  ps (b), and  $3.942$  ps (c). (d–f) Schematic of the corresponding local disorder mechanism.

states are preserved with only small changes in the peak positions and widths. In sharp contrast, at the large photoexcitation level of  $n = 7.5\%$ , at time  $t = 1$  and  $2.5$  ps, the Ge–Ge and Te–Te bond pairs show bonding characteristics, which is consistent with Ge–Ge and Te–Te wrong bond formation. That is particularly the case for Ge–Ge, which shows a well-defined peak at  $0.5$ . In the case of Te–Te, a positive tail indicates the presence of a non-negligible bonding state. In contrast, Ge–Te bond pairs, while still displaying a mostly positive bonding state, feature now a negative antibonding state tail at  $t = 1$  and  $2.5$  ps, consistent with Ge–Te bond scission. The combination of Ge–Te bond scission with Ge–Ge and some limited Te–Te bond formation is consistent with the picture of amorphization of the GeTe structure.

The results in Figures 1 and S2 indicate a threshold for the photoexcitation-induced local disorder between  $n = 4\%$  and  $5.2\%$ . It is instructive to investigate the associated disorder mechanism activated at this excitation level. Figure 3 shows the illustrations of the evolution of the structure at the local disorder site. The local structure change indicates the shift in a Ge atom position from an octahedral to a tetrahedral site in a nearest-neighbor unit cell. The transition is identified as the trigger point for the local disorder, which is also found elsewhere.<sup>7,24</sup> From Figure 3a–c, at  $t = 1.833$  ps, a Ge atom (labeled Ge1) is octahedrally bonded with six neighboring Te atoms. At  $t = 2.094$  ps, as the bond lengths between Ge1–Te5 and Ge1–Te6 atoms increase, the bonds become weaker and finally rupture. At  $t = 3.942$  ps, shown in Figure 3c, the Ge1–Te7 bond is also broken while a new Ge1–Te4 bond is formed, leading to a tetrahedrally coordinated Ge. While not shown in Figure 3, at longer times, the formation of an intermittent Ge1–Ge2 bond is also observed as the Ge1 atom moves along the  $[111]$  direction toward the Ge2 atom position. As shown in Figure 3d–f, the schematic mechanism for this Ge octahedral to tetrahedral coordination transition is proposed: (i) bond breaking with two nearest-neighbor Te atoms, (ii) motion along the  $[111]$  direction, and (iii) bond formation with diagonal Te atom with simultaneous bond breaking with another Te atom. The excited orbitals at the corresponding time are found to be concentrated in the disordered region, as plotted in Figure S7. The phase-flip mechanism proposed by Kolobov et al.<sup>20</sup> suggests that the wave function phase could be changed at high-level excitation, resulting in the weakening of GeTe longer bonds, which would

transition from bonding to antibonding states. The region with concentrated excited orbitals has a high possibility of experiencing such a phase-flip, explaining the repulsive interatomic forces leading to the observed disorder. This process is consistent with the observed increase in the MSD shown in Figure S2b. At the transition threshold, between  $4\%$  and  $5.2\%$  of valence electrons excited, the MSD values increase until the Lindemann criterion for melting is fulfilled, inducing localized nonthermal melting of the crystal structure.

Since the formation of Ge–Ge wrong bonds is observed in the disordering process, it is worth considering the bond nature in the octahedral-like to the tetrahedral-like transition of Ge coordination. We examine the homopolar Ge–Ge bonding based on crystal orbital Hamiltonian population (COHP) analysis together with the electron localization function (ELF).<sup>33</sup> A relaxed GeTe local structure at  $300$  K is shown in Figure 4a, displaying the same atoms in Figure 3. The COHP for the average Ge–Te bond in the structure is shown in Figure 4b, displaying a stable bonding state. The flat COHP curve for the Ge1–Ge2 pair and the zero ELF value between the atoms show a nonbonding state in the relaxed structure in Figures 4c and S7a. During the disorder process, the homopolar Ge1–Ge2 bond formed, as shown in Figure 4d, at  $t = 2.122$  ps. We find that the Ge–Te bonds are at a slightly antibonding state; meanwhile, the Ge1–Ge2 pair displays a weaker antibonding state, as shown in Figure 4e,f. To further understand the effect of Ge–Ge bonds in the presence of a tetrahedral structure, we consider the tetrahedral structure found at  $t = 3.942$  ps in Figure 4g. We find that the COHP for all four Ge–Te pairs is at a slight antibonding state in Figure 4h. Concurrently, Ge1–Ge2 (separated by  $2.69$  Å), Ge1–Ge3 (separated by  $2.48$  Å), and Ge1–Ge4 (separated by  $2.86$  Å) pairs show an antibonding state, as shown in Figure 4i. The evolution of the excited state with dynamic generation of bonding and antibonding states for Ge–Te and Ge–Ge pairs is one of the reasons for the swift bond-breaking after formation, as observed in our simulation.

The photoexcitation-induced amorphization process described here does not involve melting and quenching. It has been reported that the destruction of the weaker (long) Ge–Te bonds could be obtained by distorting the perfect GeTe structure, leading to a subsequent collapse of the long-range order resulting in amorphization.<sup>6</sup> The destruction of the longer bonds is induced by photoexciting electrons from high-energy states in the valence band to low-energy states in the

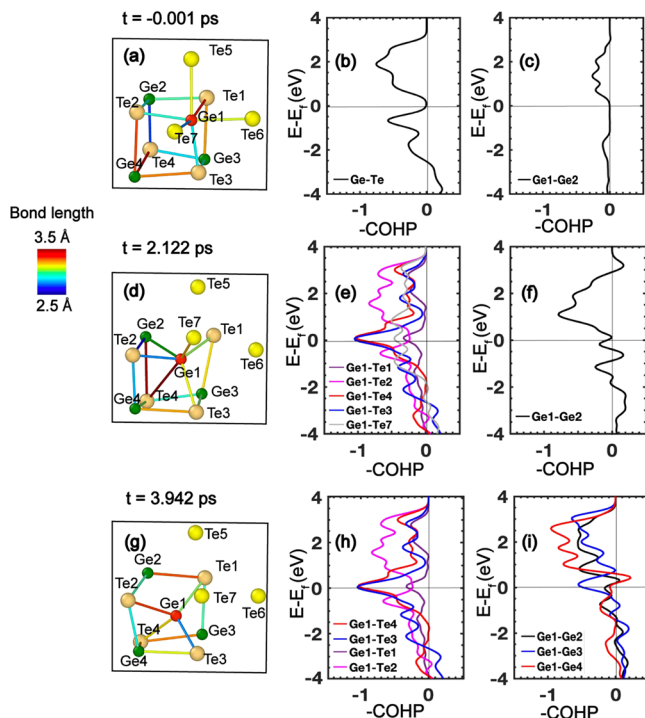


**Figure 4.** COHP bonding analysis of Ge–Te and Ge–Ge interaction. (a–c) Bond length (a) and COHP (b and c) before Ge1–Ge2 bond formation for  $t = -0.001$  ps. (d–f) Bond length (d) and COHP (e and f) after Ge–Ge bond formation for  $t = 2.122$  ps. (g–i) Bond length (g) and COHP (h and i) after Ge–Ge bond formation for  $t = 3.942$  ps.

conduction band, enhancing the concentration of non-equilibrium charge carriers. These charge carriers populate antibonding states of the weaker metavalent bonds,<sup>34</sup> as shown in the COHP curves in Figure S6, leading to structural relaxation and bond rupture, causing the collapse of the long-

range order. This mechanism effectively opens a path for lowering the energy barrier for bond breaking and triggering structural disorder at a temperature lower than the nominal melting point, similar to photoexcitation preferential bond rupture in  $\text{As}_2\text{S}_3$ <sup>35</sup> and GST.<sup>36</sup>

Figures 2 and 4 show that Ge–Ge bonding does not lead to strong antibonding states. Otherwise, Ge–Ge bonding would result in a large repulsive force, which would be unfavorable for the approximation and bond formation between Ge1 and Ge2 atoms. Furthermore, with proper Ge–Ge distance, the bonding state of Ge–Ge pairs is reported in the disordered region, supporting its stability. These results are supported by bond-weighted distribution function calculations,<sup>37</sup> showing that Ge–Ge bonds are chemically stronger in tetrahedral motifs than in octahedral motifs. It is also suggested that the unexpected Ge–Ge bonding interactions support the reshuffling of electrons from antibonding Ge–Te into bonding Ge–Ge contacts, lowering the energy and enhancing the stability of the structure.<sup>38</sup>

The results in Figure 5 show the change in the Kohn–Sham energy eigenvalues and provide visualizations of the excited orbitals as a function of simulation time. After excitation at  $n = 4.0\%$ , the appearance of the singly occupied orbitals, as shown in Figure 5a, is a consequence of the evolution of the excited state. The decline of the blue and yellow lines in Figure 5a shows the partial recovery of the ground state within the 4.5 ps of simulation. Figure 5b–d shows the concentration of excited high-energy orbitals in the locally disordered region.

In summary, by performing NAQMD simulations, a nonthermal structural disorder in GeTe occurs after photoexcitation at an excitation level of no less than 4.0%. Accompanying the photoexcitation is the swift charge transfer from Te to Ge atoms. The Mulliken bond overlap shows increased Ge–Ge and Te–Te bonding interaction with weakened Ge–Te bonding interaction. The examination of local disorder at 4.0% excitation level shows the trigger to be a Ge atom diffusion from octahedral to tetrahedral sites.

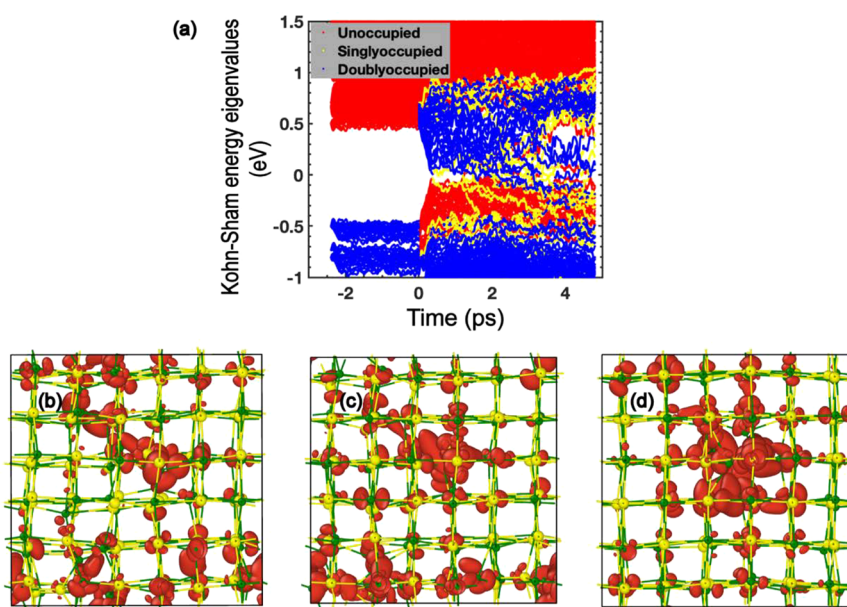


**Figure 5.** Evolution of Kohn–Sham energy eigenvalues and the excited orbitals for photoexcitation level  $n = 4.0\%$ . (a) Kohn–Sham energy eigenvalues as a function of time. The red, yellow, and blue curves represent orbitals that are empty, singly occupied, and doubly occupied, respectively. (b–d) Excited orbitals for  $t = 1.833$  ps (b),  $2.094$  ps (c), and  $3.942$  ps (d).

Meanwhile, the excited orbitals are found to be concentrated in the locally disordered region. This work sheds light on structural and electronic mechanisms for photoexcitation-induced GeTe amorphization and explores the bonding nature during this process.

## METHODS

NAQMD simulations are performed on a supercell composed of  $3 \times 3 \times 3$  cubic GeTe crystalline unit cells with lattice constant  $a = b = c = 6 \text{ \AA}$ , containing a total of 216 atoms. The system is first relaxed in a canonical ensemble at a temperature of  $T = 300 \text{ K}$  using a Nosé–Hoover thermostat.<sup>39</sup> The  $\Gamma$  point is used to sample the Brillouin zone. NAQMD simulations are then performed in a canonical ensemble at  $T = 700 \text{ K}$ . A time step of 1.2 fs is used in the integration of the equations of motion. All simulations are performed using the plane-wave basis quantum molecular dynamics code QXMD.<sup>40,41</sup>

In quantum molecular dynamics, the trajectories of all atoms are integrated based on interatomic forces calculated using the Hellmann–Feynman theorem in the density functional theory framework.<sup>42–45</sup> The GGA-PBE approximation is employed for the exchange–correlation energy, and dispersion forces are calculated with the DFT-D correction method.<sup>46,47</sup> The projector augmented wave (PAW) method is used in the calculation of the electronic states.<sup>48</sup> The plane-wave cutoff energy is set at 30 Ry for the electronic wave functions and 250 Ry for the electronic charge density. The dynamics of the excited states is modeled using the fewest-switches-surface-hopping method.<sup>41,49,50</sup> In NAQMD, excited-state forces are computed using an extension of the Harris–Foulkes approach.<sup>41</sup> Details of the NAQMD method are reported elsewhere.<sup>41</sup>

## ASSOCIATED CONTENT

### Data Availability Statement

Data available on request from the authors.

### Supporting Information

The Supporting Information is available free of charge at <https://pubs.acs.org/doi/10.1021/acs.jpcllett.2c02448>.

Ge–Te bond length distribution before and after thermalization at 300 K; mean square displacement and the fraction of wrong bonds; density of states (DOS) of GeTe during amorphization for photoexcitation level  $n = 4.0\%$ ; evolution of Kohn–Sham energy eigenvalues for photoexcitation level  $n = 4.0\%$ ; average Mulliken charge as a function of time for different photoexcitation levels; evolution of the excited orbitals; COHP bonding analysis of Ge1–Te5 and Ge1–Te6 interaction; ELF analysis of Ge–Te and Ge–Ge interaction ([PDF](#))

## AUTHOR INFORMATION

### Corresponding Author

Paulo S. Branicio — Mork Family Department of Chemical Engineering and Materials Science, University of Southern California, Los Angeles, California 90089, United States; [orcid.org/0000-0002-8676-3644](#); Email: [branicio@usc.edu](mailto:branicio@usc.edu)

## Authors

Liqiu Yang — Collaboratory for Advanced Computing and Simulation, University of Southern California, Los Angeles, California 90089, United States

Subodh C. Tiwari — Collaboratory for Advanced Computing and Simulation, University of Southern California, Los Angeles, California 90089, United States; [orcid.org/0000-0002-5516-6900](#)

Shogo Fukushima — Department of Physics, Kumamoto University, Kumamoto 860-8555, Japan

Fuyuki Shimojo — Department of Physics, Kumamoto University, Kumamoto 860-8555, Japan

Rajiv K. Kalia — Collaboratory for Advanced Computing and Simulation, University of Southern California, Los Angeles, California 90089, United States

Aiichiro Nakano — Collaboratory for Advanced Computing and Simulation, University of Southern California, Los Angeles, California 90089, United States; [orcid.org/0000-0003-3228-3896](#)

Priya Vashishta — Collaboratory for Advanced Computing and Simulation, University of Southern California, Los Angeles, California 90089, United States; [orcid.org/0000-0003-4683-429X](#)

Complete contact information is available at:

<https://pubs.acs.org/10.1021/acs.jpcllett.2c02448>

## Author Contributions

Conceptualization: S.C.T., P.S.B.; Methodology: F.S., A.N.; Investigation: L.Y., S.C.T., S.F.; Visualization: L.Y., S.C.T.; Supervision: R.K.K., A.N., P.V., P.S.B.; Writing—original draft: L.Y.; Writing—review and editing: P.S.B., A.N.

## Notes

The authors declare no competing financial interest.

## ACKNOWLEDGMENTS

This work was supported as part of the Computational Materials Sciences Program funded by the U.S. Department of Energy, Office of Science, Basic Energy Sciences, under Award DE-SC0014607. A.N. was supported by the National Science Foundation, Award OAC 2118061. We would also like to acknowledge the University of Southern California Center for Advanced Research Computing (USC-CARC) and the Argonne Leadership Computing Facility under the DOE INCITE and Aurora Early Science Programs for providing computing resources.

## REFERENCES

- (1) Wuttig, M.; Yamada, N. Phase-Change Materials for Rewriteable Data Storage. *Nat. Mater.* **2007**, *6*, 824–832.
- (2) Kolobov, A. V.; Tominaga, J. *Chalcogenides: Metastability and Phase Change Phenomena*; Springer Science & Business Media, 2012; Vol. 164.
- (3) Deringer, V. L.; Dronskowski, R.; Wuttig, M. Microscopic Complexity in Phase-Change Materials and Its Role for Applications. *Adv. Funct. Mater.* **2015**, *25*, 6343–6359.
- (4) Branicio, P. S.; Bai, K.; Ramanarayanan, H.; Wu, D. T.; Sullivan, M. B.; Srolovitz, D. J. Atomistic Insights into the Nanosecond Long Amorphization and Crystallization Cycle of Nanoscale  $\text{Ge}_2\text{Sb}_2\text{Te}_5$ : An Ab Initio Molecular Dynamics Study. *Phys. Rev. Mater.* **2018**, *2*, 043401.
- (5) Song, Z.; Wang, R.; Xue, Y.; Song, S. The “Gene” of Reversible Phase Transformation of Phase Change Materials: Octahedral Motif. *Nano Res.* **2022**, *15*, 765–772.

- (6) Kolobov, A. V.; Krabal, M.; Fons, P.; Tominaga, J.; Uruga, T. Distortion-Triggered Loss of Long-Range Order in Solids with Bonding Energy Hierarchy. *Nat. Chem.* **2011**, *3*, 311–316.
- (7) Li, X.-B.; Liu, X. Q.; Liu, X.; Han, D.; Zhang, Z.; Han, X. D.; Sun, H.-B.; Zhang, S. B. Role of Electronic Excitation in the Amorphization of Ge-Sb-Te Alloys. *Phys. Rev. Lett.* **2011**, *107*, 015501.
- (8) Tiwari, S. C.; Kalia, R. K.; Nakano, A.; Shimojo, F.; Vashishta, P.; Branicio, P. S. Photoexcitation Induced Ultrafast Nonthermal Amorphization in  $Sb_2Te_3$ . *J. Phys. Chem. Lett.* **2020**, *11*, 10242–10249.
- (9) Matsubara, E.; et al. Initial Atomic Motion Immediately Following Femtosecond-Laser Excitation in Phase-Change Materials. *Phys. Rev. Lett.* **2016**, *117*, 135501.
- (10) Bruns, G.; Merkelbach, P.; Schlockermann, C.; Salinga, M.; Wuttig, M.; Happ, T. D.; Philipp, J. B.; Kund, M. Nanosecond Switching in GeTe Phase Change Memory Cells. *Appl. Phys. Lett.* **2009**, *95*, 043108.
- (11) Singh, K.; Kumari, S.; Singh, H.; Bala, N.; Singh, P.; Kumar, A.; Thakur, A. A Review on GeTe Thin Film-Based Phase-Change Materials. *Appl. Nanosci.* **2021**. DOI: 10.1007/s13204-021-01911-7
- (12) Da Silva, J. L. F.; Walsh, A.; Lee, H. Insights into the Structure of the Stable and Metastable  $(GeTe)_m(Sb_2Te_3)_n$  Compounds. *Phys. Rev. B* **2008**, *78*, 224111.
- (13) Lucovsky, G.; White, R. M. Effects of Resonance Bonding on the Properties of Crystalline and Amorphous Semiconductors. *Phys. Rev. B* **1973**, *8*, 660–667.
- (14) Robertson, J.; Xiong, K.; Peacock, P. W. Electronic and Atomic Structure of  $Ge_2Sb_2Te_5$  Phase Change Memory Material. *Thin Solid Films* **2007**, *515*, 7538–7541.
- (15) Lencer, D.; Salinga, M.; Wuttig, M. Design Rules for Phase-Change Materials in Data Storage Applications. *Adv. Mater.* **2011**, *23*, 2030–2058.
- (16) Caravati, S.; Bernasconi, M.; Kühne, T. D.; Krack, M.; Parrinello, M. Coexistence of Tetrahedral- and Octahedral-Like Sites in Amorphous Phase Change Materials. *Appl. Phys. Lett.* **2007**, *91*, 171906.
- (17) Akola, J.; Jones, R. O. Structural Phase Transitions on the Nanoscale: The Crucial Pattern in the Phase-Change Materials  $GeSbTe_5$  and GeTe. *Phys. Rev. B* **2007**, *76*, 235201.
- (18) Hegedüs, J.; Elliott, S. R. Microscopic Origin of the Fast Crystallization Ability of Ge–Sb–Te Phase-Change Memory materials. *Nat. Mater.* **2008**, *7*, 399–405.
- (19) Krabal, M.; Kolobov, A. V.; Fons, P.; Tominaga, J.; Elliott, S. R.; Hegedüs, J.; Uruga, T. Intrinsic Complexity of the Melt-Quenched Amorphous  $Ge_2Sb_2Te_5$  Memory Alloy. *Phys. Rev. B* **2011**, *83*, 054203.
- (20) Kolobov, A. V.; Fons, P.; Frenkel, A. I.; Ankudinov, A. L.; Tominaga, J.; Uruga, T. Understanding the Phase-Change Mechanism of Rewritable Optical Media. *Nat. Mater.* **2004**, *3*, 703–708.
- (21) Paesler, M. A.; Baker, D. A.; Lucovsky, G.; Edwards, A. E.; Taylor, P. C. EXAFS Study of Local Order in the Amorphous Chalcogenide Semiconductor  $Ge_2Sb_2Te_5$ . *J. Phys. Chem. Solids* **2007**, *68*, 873–877.
- (22) Kolobov, A. V.; Fons, P.; Tominaga, J.; Hase, M. Excitation-Assisted Disordering of GeTe and Related Solids with Resonant Bonding. *J. Phys. Chem. C* **2014**, *118*, 10248–10253.
- (23) Wautelet, M. Cohesion of Solids under Very High Electronic Excitation Conditions. *Phys. Status Solidi* **1986**, *138*, 447–456.
- (24) Sundaram, S. K.; Mazur, E. Inducing and Probing Non-Thermal Transitions in Semiconductors Using Femtosecond Laser Pulses. *Nat. Mater.* **2002**, *1*, 217–224.
- (25) Kolobov, A. V.; Fons, P.; Tominaga, J. Understanding Phase-Change Memory Alloys from a Chemical Perspective. *Sci. Rep.* **2015**, *5*, 13698.
- (26) Yamada, N.; Matsunaga, T. Structure of Laser-Crystallized  $Ge_2Sb_{2+x}Te_5$  Sputtered Thin Films for Use in Optical Memory. *J. Appl. Phys.* **2000**, *88*, 7020–7028.
- (27) Shamoto, S.; Yamada, N.; Matsunaga, T.; Proffen, T.; Richardson, J. W.; Chung, J. H.; Egami, T. Large Displacement of Germanium Atoms in Crystalline  $Ge_2Sb_2Te_5$ . *Appl. Phys. Lett.* **2005**, *86*, 081904.
- (28) Shayduk, R.; Braun, W. Epitaxial Films for Ge–Sb–Te Phase Change Memory. *J. Cryst. Growth* **2009**, *311*, 2215–2219.
- (29) Welnic, W.; Pamungkas, A.; Detemple, R.; Steimer, C.; Blügel, S.; Wuttig, M. Unravelling the Interplay of Local Structure and Physical Properties in Phase-Change Materials. *Nat. Mater.* **2006**, *5*, 56–62.
- (30) Kolobov, A. V.; Fons, P.; Tominaga, J.; Frenkel, A. I.; Ankudinov, A. L.; Yannopoulos, S. N.; Andrikopoulos, K. S.; Uruga, T. Why Phase-Change Media Are Fast and Stable: A New Approach to an Old Problem. *Japanese journal of applied physics* **2005**, *44*, 3345.
- (31) Cornwell, J. F. *Group Theory and Electronic Energy Bands in Solids*; North-Holland Amsterdam, 1969.
- (32) Deringer, V. L.; Tchougréeff, A. L.; Dronskowski, R. Crystal Orbital Hamilton Population (COHP) Analysis as Projected from Plane-Wave Basis Sets. *J. Phys. Chem. A* **2011**, *115*, 5461–5466.
- (33) Savin, A.; Nesper, R.; Wengert, S.; Fässler, T. F. ELF: The Electron Localization Function. *Angew. Chem. Int. Ed.* **1997**, *36*, 1808–1832.
- (34) Kerres, P.; et al. Scaling and Confinement in Ultrathin Chalcogenide Films as Exemplified by GeTe. *Small* **2022**, *18*, 2201753.
- (35) Yannopoulos, S. N.; Trunov, M. L. Photoplastic Effects in Chalcogenide Glasses: A Review. *Phys. Status Solidi* **2009**, *246*, 1773–1785.
- (36) Fons, P.; Osawa, H.; Kolobov, A.; Fukaya, T.; Suzuki, M.; Uruga, T.; Kawamura, N.; Tanida, H.; Tominaga, J. Photoassisted Amorphization of the Phase-Change Memory Alloy  $Ge_2Sb_2Te_5$ . *Phys. Rev. B* **2010**, *82*, 041203.
- (37) Deringer, V. L.; Zhang, W.; Lumeij, M.; Maintz, S.; Wuttig, M.; Mazzarello, R.; Dronskowski, R. Bonding Nature of Local Structural Motifs in Amorphous GeTe. *Angew. Chem., Int. Ed.* **2014**, *53*, 10817–10820.
- (38) KüPers, M.; et al. Unexpected Ge–Ge Contacts in the Two-Dimensional  $Ge_4Se_3Te$  Phase and Analysis of Their Chemical Cause with the Density of Energy (DOE) Function. *Angew. Chem., Int. Ed.* **2017**, *56*, 10204–10208.
- (39) Nosé, S. A Molecular Dynamics Method for Simulations in the Canonical Ensemble. *Mol. Phys.* **1984**, *52*, 255–268.
- (40) Shimojo, F.; et al. QXMD: An Open-Source Program for Nonadiabatic Quantum Molecular Dynamics. *SoftwareX* **2019**, *10*, 100307.
- (41) Shimojo, F.; Ohmura, S.; Mou, W.; Kalia, R. K.; Nakano, A.; Vashishta, P. Large Nonadiabatic Quantum Molecular Dynamics Simulations on Parallel Computers. *Comput. Phys. Commun.* **2013**, *184*, 1–8.
- (42) Hohenberg, P.; Kohn, W. Inhomogeneous Electron Gas. *Phys. Rev.* **1964**, *136*, B864–B871.
- (43) Car, R.; Parrinello, M. Unified Approach for Molecular Dynamics and Density-Functional Theory. *Phys. Rev. Lett.* **1985**, *55*, 2471–2474.
- (44) Kohn, W.; Sham, L. J. Self-Consistent Equations Including Exchange and Correlation Effects. *Phys. Rev.* **1965**, *140*, A1133–A1138.
- (45) Kohn, W.; Vashishta, P. General Density Functional Theory. In *Theory of the Inhomogeneous Electron Gas*; Lundqvist, S., March, N. H., Eds.; Springer US: Boston, MA, 1983; pp 79–147.
- (46) Perdew, J. P.; Burke, K.; Ernzerhof, M. Generalized Gradient Approximation Made Simple. *Phys. Rev. Lett.* **1996**, *77*, 3865–3868.
- (47) Grimme, S. Semiempirical GGA-Type Density Functional Constructed with a Long-Range Dispersion Correction. *J. Comput. Chem.* **2006**, *27*, 1787–1799.
- (48) Blöchl, P. E. Projector Augmented-Wave Method. *Phys. Rev. B* **1994**, *50*, 17953–17979.
- (49) Tully, J. C. Molecular Dynamics with Electronic Transitions. *J. Chem. Phys.* **1990**, *93*, 1061–1071.

(50) Casida, M. E.; Chong, D. *Recent Advances in Density Functional Methods: Computational Chemistry: Reviews of Current Trends* **1995**, 155 DOI: 10.1142/9789812830586\_0005.